

**NANO EXPRESS**

**Open Access**



# Fabrication and Properties of High-Efficiency Perovskite/PCBM Organic Solar Cells

Lung-Chien Chen<sup>1\*</sup>, Jhih-Chyi Chen<sup>1</sup>, Cheng-Chiang Chen<sup>2</sup> and Chun-Guey Wu<sup>2</sup>

## Abstract

This work presents a  $\text{CH}_3\text{NH}_3\text{PbI}_3/\text{PCBM}$  organic solar cell. Organic PCBM film and  $\text{CH}_3\text{NH}_3\text{PbI}_3$  perovskite film are deposited on the PEDOT:PSS/ITO glass substrate by the spin coating method. The performance of the organic solar cells was observed by changing the thickness of  $\text{CH}_3\text{NH}_3\text{PbI}_3$  perovskite. The thickness of a perovskite film can affect the carrier diffusion length in a device that strongly absorbs light in the red spectral region. The short-circuit current density and the power conversion efficiency were  $21.9 \text{ mA/cm}^2$  and 11.99 %, respectively, for the sample with 210-nm-thick  $\text{CH}_3\text{NH}_3\text{PbI}_3$  perovskite active layer.

**Keywords:** XRD; Absorption; Organic solar cells;  $\text{CH}_3\text{NH}_3\text{PbI}_3$  perovskite

## Background

Perovskite solar cell has attracted considerable attention because of its unique properties and potential applications. As the hybrid organic/inorganic lead halide perovskite (e.g.,  $\text{CH}_3\text{NH}_3\text{PbX}_3$ ,  $X = \text{I, Cl, Br}$ ) materials, perovskite has a high absorption coefficient, long hole–electron diffusion length ( $\sim 0.1\text{--}1 \mu\text{m}$ ), tunable band gaps, and good carrier transport [1–20]. The perovskite and its derivatives have been achieved in various types of solar cell architectures including perovskite-sensitized solar cells, mesoporous (mp)- $\text{TiO}_2$ /perovskite material, and planar p–i–n heterojunction solar cells [21–24]. However,  $\text{CH}_3\text{NH}_3\text{PbI}_3$  perovskite films can be prepared by dual-source thermal evaporation system [25], vapor-assisted solution process [26], and one-step and two-step spin coating procedures for  $\text{CH}_3\text{NH}_3\text{PbI}_3$  formation [27, 28] which has many advantages such as low cost, low temperature, and ease of control.

In this work, we report the solution process fabrication of perovskite solar cells which comprised an architecture  $\text{CH}_3\text{NH}_3\text{PbI}_3$  perovskites formed by a solvent-engineering technology. This study investigated the optical, structural, and surface properties of a perovskite film that is grown on PEDOT:PSS/ITO electrodes by the solvent-engineering

technology as functions of thickness in high-performance perovskite solar cells.

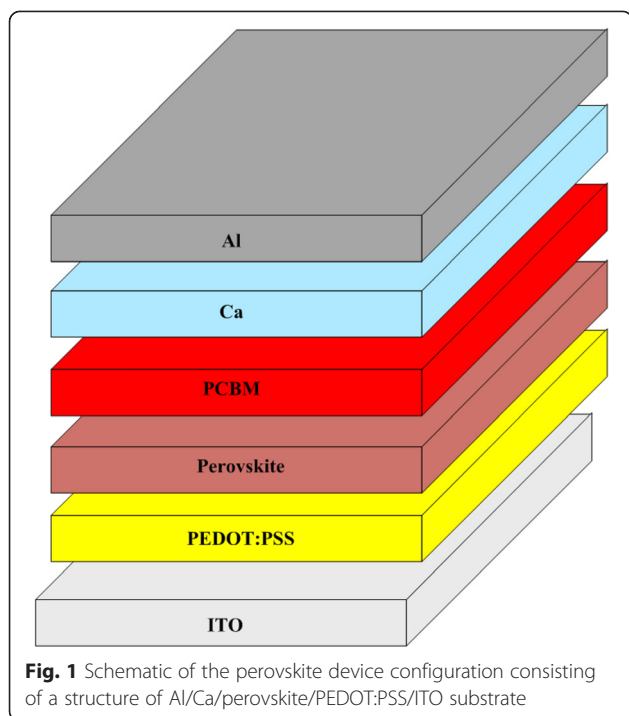
## Methods

In this study, a PEDOT:PSS (CLEVIOS Al 4083) film was spin-coated on a pre-cleaned ITO substrate at 5000 rpm for 30 s. After spin coating, the film was annealed at  $140 \text{ }^\circ\text{C}$  for 10 min. The perovskite layer was deposited by the solvent-engineering technology of 1.2 M  $\text{PbI}_2$  and 1.2 M methylammonium iodide (MAI) in a cosolvent of dimethyl sulfoxide (DMSO) and  $\gamma$ -butyrolactone (GBL) (vol. ratio = 1:1) in a glove box filled with highly pure nitrogen. The perovskite solutions were then coated onto the PEDOT:PSS/ITO substrate by two consecutive spin coating steps, at 1000 and 5000 rpm for 10 and 20 s, respectively. At 5000 rpm for 20 s, the wet spinning film was quenched by dropping  $50 \mu\text{l}$  of anhydrous toluene. After spin coating, the film was annealed at  $100 \text{ }^\circ\text{C}$  for 10 min. A solution of PCBM was spin-coated on the perovskite layer/PEDOT:PSS/ITO substrate at 3000 rpm for 30 s. Finally, a Ca/Al electrode was completed by thermal deposition with a thickness of 100 nm. Figure 1 schematically depicts the complete structure. The roles of the PCBM film,  $\text{CH}_3\text{NH}_3\text{PbI}_3$  film, and PEDOT:PSS film in the cell structure is electron transport layer, active layer, and hole transport layer, respectively.

A field emission scanning electron microscope (FESEM) (LEO 1530) was used to observe the cross section and

\* Correspondence: ocean@ntut.edu.tw

<sup>1</sup>Department of Electro-Optical Engineering, National Taipei University of Technology, 1, Section 3, Chung-Hsiao E. Road, Taipei 106, Taiwan  
Full list of author information is available at the end of the article



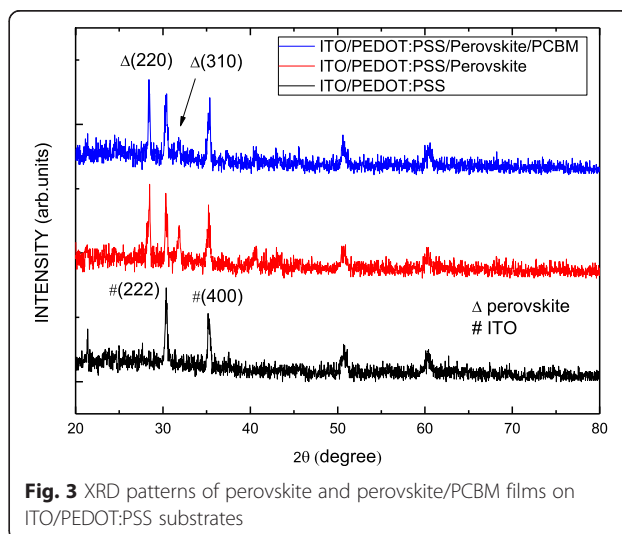
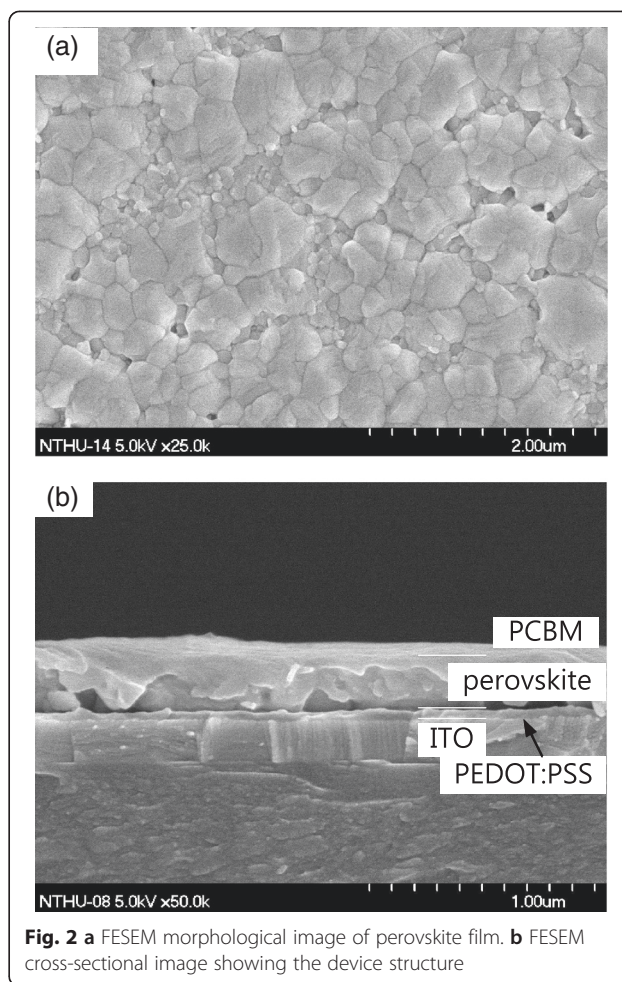
surface morphology of the cells. Moreover, the current density–voltage ( $J$ – $V$ ) characteristics were measured using a Keithley 2420 programmable source meter under irradiation by a 1000-W xenon lamp. Finally, the irradiation power density on the surface of the sample was calibrated as 1000 W/m<sup>2</sup>.

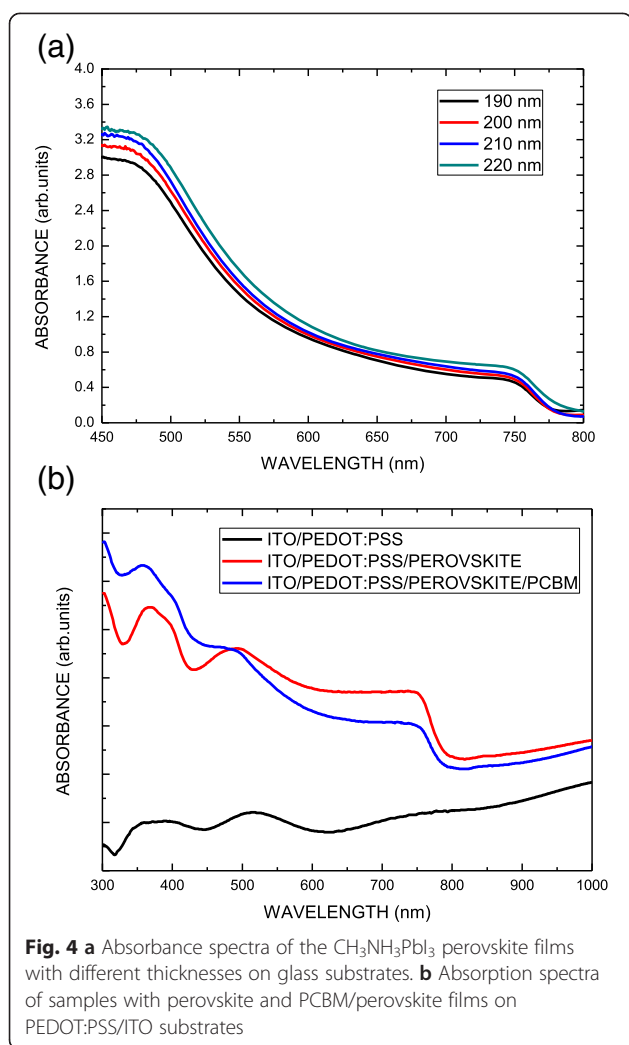
## Results and Discussion

Figure 2a, b presents the cross-sectional and surface FESEM images of the perovskite films on glass substrate. Perovskite prepared by the one-step coating method shows cuboid-like crystals, the average CH<sub>3</sub>NH<sub>3</sub>PbI<sub>3</sub> crystal size from about 200 nm to about 600 nm, as shown in Fig. 2a. A high-resolution image of the cross section of the obtained perovskite solar cell configuration is shown in Fig. 2b. It clearly indicates the presence of each layer of ITO (200 nm), PEDOT:PSS (~50 nm), perovskite (~200 nm), and PCBM (~80 nm).

Figure 3 shows the XRD patterns of CH<sub>3</sub>NH<sub>3</sub>PbI<sub>3</sub> and PCBM/CH<sub>3</sub>NH<sub>3</sub>PbI<sub>3</sub> perovskite films deposited on PEDOT:PSS/ITO substrates. The spectra in this study reveal two peaks at the position of 28.39° and 31.86°, which correlate well with (220) and (310) planes of the CH<sub>3</sub>NH<sub>3</sub>PbI<sub>3</sub> perovskite phase. This result suggests that the solvent in the PCBM film does not destroy the structure of the underlying CH<sub>3</sub>NH<sub>3</sub>PbI<sub>3</sub> perovskite film during the coating.

Figure 4 plots the UV-visible absorption measurements. Figure 4a shows the absorbance spectra of the





$\text{CH}_3\text{NH}_3\text{PbI}_3$  perovskite films with different thicknesses on glass substrates. The  $\text{CH}_3\text{NH}_3\text{PbI}_3$  perovskite film with 190-nm thickness is lower than that of the film with 220-nm thickness. In other words, more sunlight can be absorbed to generate excitons in the perovskite film when the thickness increases. Figure 4b shows the absorption spectra of samples with perovskite and PCBM/perovskite films on PEDOT:PSS/ITO substrates. The samples yielded the typical absorption spectrum of  $\text{CH}_3\text{NH}_3\text{PbI}_3$  perovskite between 300 and 760 nm due to the band gap of 1.6 eV [29]. As seen, the absorption of PEDOT:PSS/ITO glass substrate in the presence of  $\text{CH}_3\text{NH}_3\text{PbI}_3$ , was significantly enhanced throughout the visible region, confirming the possibility of the contribution of  $\text{CH}_3\text{NH}_3\text{PbI}_3$  to the harvesting of light. To compare with the sample of  $\text{CH}_3\text{NH}_3\text{PbI}_3$  on PEDOT:PSS/ITO substrate, for the sample of PCBM/ $\text{CH}_3\text{NH}_3\text{PbI}_3$  on PEDOT:PSS/ITO

substrate, the absorption of wavelengths in the range 300–500 nm lightly increases, and the absorption of wavelengths in the range 500–760 nm lightly decreases. That may be attributed to the PCBM absorption [30].

Figure 5 plots photocurrent  $J$ - $V$  curves of the perovskite solar cell obtained under  $100 \text{ mW}/\text{cm}^2$  illumination and the AM1.5G condition. The cell has an active area of  $5 \times 5 \text{ mm}^2$  and no antireflective coating. Table 1 lists the main characteristics of those samples. According to Table 1, the series resistance ( $R_s$ ) of cell increases when the thickness of the  $\text{CH}_3\text{NH}_3\text{PbI}_3$  perovskite film increases, and the thickness of the  $\text{CH}_3\text{NH}_3\text{PbI}_3$  perovskite film can affect the carrier diffusion length in a device that strongly absorbs light in the red spectral region. The perovskite solar cell fabricated on the 210-nm-thick perovskite film showed the highest power conversion efficiency (EFF),  $\eta = 11.99 \%$  value ( $J_{sc} = 21.9 \text{ mA}/\text{cm}^2$ ) due to increased photocurrent density. From the  $J$ - $V$  curve and  $\eta$  value, we can decide that the optimized passivating thickness of the perovskite film is 210 nm thick. However, further increase in thickness of the perovskite film to 220 nm resulted in decrease of  $\eta = 9.88 \%$  value ( $J_{sc} = 22 \text{ mA}/\text{cm}^2$ ). Therefore, a film of optimal thickness would absorb more light and yield a higher current.

Figure 6 presents the photoluminescence (PL) spectra of the  $\text{CH}_3\text{NH}_3\text{PbI}_3$  perovskite films with different thicknesses on glass substrates. The dominant peak located at 1.615 eV (768 nm) corresponds to the optical band gap of the  $\text{CH}_3\text{NH}_3\text{PbI}_3$  perovskite films with a direct band gap and can be attributed to the recombination of the near band-to-band (B-B) [29]. When the thickness of the  $\text{CH}_3\text{NH}_3\text{PbI}_3$  perovskite film increases, the PL intensity increases. However, under identical experimental conditions, the PL quantum yield of the 220-nm-thick  $\text{CH}_3\text{NH}_3\text{PbI}_3$  is greatly reduced. Therefore, it was

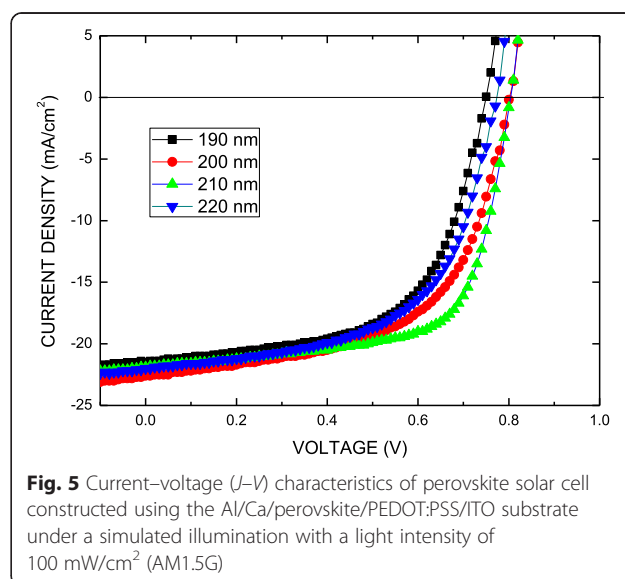


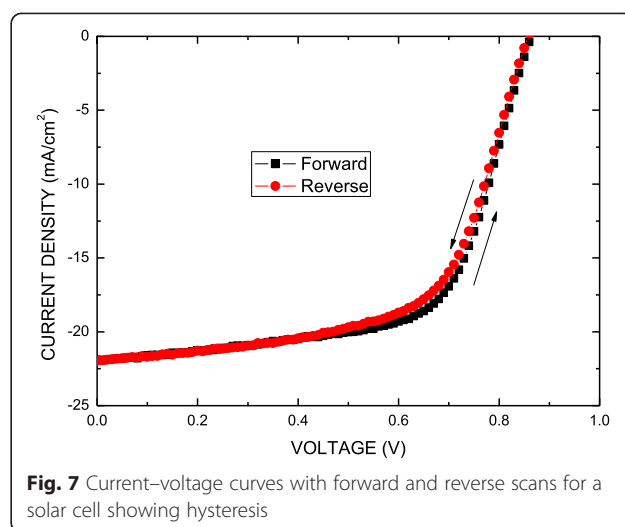
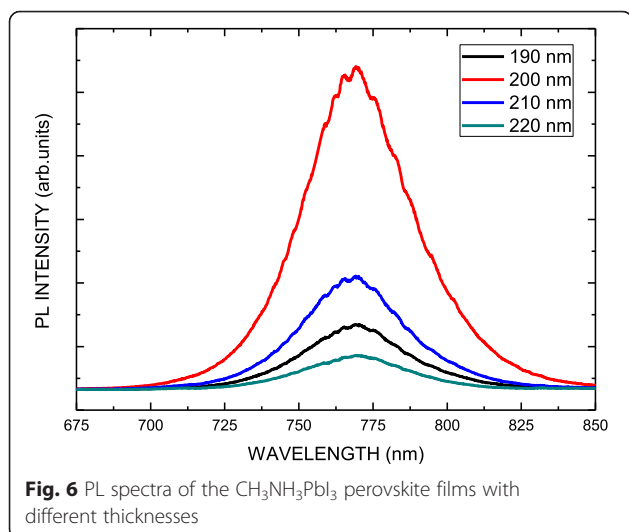
**Table 1** Measurements of all samples in this study

Thickness (nm)	$J_{sc}$ (mA/cm <sup>2</sup> )	$V_{oc}$ (V)	FF	Efficiency (%)	$R_s$ ( $\Omega$ )
190	21.5	0.75	0.595	9.59	3.9
200	22.6	0.81	0.579	10.60	4.4
210	21.9	0.81	0.676	11.99	4.7
220	22.0	0.77	0.583	9.88	4.8

found that a more strikingly quenching effect was in the 220-nm-thick perovskite layer than in the 200-nm-thick perovskite layer.

The hysteresis effect in the perovskite-based solar cells was reported [31–34]. The reasons may include the collection of excess carrier, defects in materials, ion movement caused by polarization, or ferroelectric effects. Figure 7 shows the current–voltage curves with forward and reverse scans for a solar cell showing hysteresis. The scan parameters are scan speed (0.2 V/s) and delay time (40 ms). As shown in Fig. 7, a hysteresis was observed in the  $J$ – $V$  curves of the present cell, 12.04 and 11.52 % for the forward and reverse bias scans. Only a 0.52 % drop in efficiency was observed as compared to that in the forward bias scan. The average values from the  $J$ – $V$  curves in reverse and forward scans exhibited a  $J_{sc}$  of 21.925 mA/cm<sup>2</sup>,  $V_{oc}$  of 0.86 V, and FF of 62.5 %, corresponding to a PCE of 11.78 % under standard AM1.5G conditions.

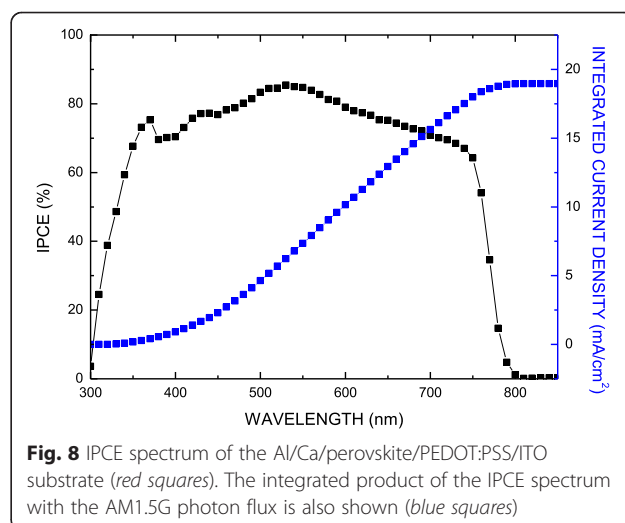
Figure 8 displays incident photon-to-electron conversion efficiency (IPCE) spectrum of the Al/Ca/perovskite/PEDOT:PSS/ITO substrate (red squares). The integrated product of the IPCE spectrum with the AM1.5G photon flux is also shown (blue squares). The IPCE spectrum shows the expected behavior for a high-performance device based on CH<sub>3</sub>NH<sub>3</sub>PbI<sub>3</sub>. The onset of photocurrent at 800 nm is consistent with the reported band gap of CH<sub>3</sub>NH<sub>3</sub>PbI<sub>3</sub> [29]. The best device also showed a very



broad IPCE plateau of over 80 % between 480 and 600 nm, as shown in Fig. 8. Integrating the product of the AM1.5G photon flux with the IPCE spectrum yields a predicted  $J_{sc}$  of around 19 mA/cm<sup>2</sup>, which is in agreement with the measured value of around 22 mA/cm<sup>2</sup>.

## Conclusions

High-efficiency and low-cost perovskite/PCBM organic solar cells with various thicknesses of CH<sub>3</sub>NH<sub>3</sub>PbI<sub>3</sub> perovskite were fabricated. The PCBM film as the electron transport layer in the cell structure can improve the optical absorption in the wavelength range of 300–500 nm, and the absorption in the wavelength range of 500–760 nm is lightly dropped according to the comparison between the samples of PCBM/CH<sub>3</sub>NH<sub>3</sub>PbI<sub>3</sub> on substrate and CH<sub>3</sub>NH<sub>3</sub>PbI<sub>3</sub> on substrate. The short-circuit current density and the power conversion efficiency were 21.9 mA/cm<sup>2</sup> and 11.99 %, respectively, for the



## optimal measured parameters of the sample with 210-nm-thick $\text{CH}_3\text{NH}_3\text{PbI}_3$ perovskite.

### Competing Interests

The authors declare that they have no competing interests.

### Authors' Contributions

LCC wrote the paper, designed the experiments, and analyzed the data. JCC and CCC prepared the samples and did all the measurements. CGW made the discussion and suggested the parameters. All authors read and approved the final manuscript.

### Acknowledgements

Financial support of this paper was provided by the Ministry of Science and Technology of the Republic of China under Contract No. NSC 103-2221-E-027-029-MY2.

### Author details

<sup>1</sup>Department of Electro-Optical Engineering, National Taipei University of Technology, 1, Section 3, Chung-Hsiao E. Road, Taipei 106, Taiwan. <sup>2</sup>Research Center for New Generation Photovoltaics, National Central University, Taoyuan 32001, Taiwan.

Received: 11 May 2015 Accepted: 25 July 2015

Published online: 05 August 2015

### References

- Stoumpos CC, Malliakas CD, Kanatzidis MG. Semiconducting tin and lead iodide perovskites with organic cations: phase transitions, high mobilities, and near-infrared photoluminescent properties. *Inorg Chem*. 2013;52:9019–38.
- Snaith HJ. Perovskites: the emergence of a new era for low-cost, high-efficiency solar cells. *J Phys Chem Lett*. 2013;4:3623–30.
- Noh JH, Im SH, Heo JH, Mandal TN, Seok SI. Chemical management for colorful, efficient, and stable inorganic–organic hybrid nanostructured solar cells. *Nano Lett*. 2013;13:1764–9.
- Hao F, Stoumpos CC, Chang RPH, Kanatzidis MG. Anomalous band gap behavior in mixed Sn and Pb perovskites enables broadening of absorption spectrum in solar cells. *J Am Chem Soc*. 2014;136:8094–9.
- Liang K, Mitzi DB, Prikas MT. Synthesis and characterization of organic–inorganic perovskite thin films prepared using a versatile two-step dipping technique. *Chem Mater*. 1998;10:403–11.
- Kojima A, Teshima K, Shirai Y, Miyasaka T. Organometal halide perovskites as visible-light sensitizers for photovoltaic cells. *J Am Chem Soc*. 2009;131:6050–1.
- Im JH, Lee CR, Lee JW, Park SW, Park NG. 6.5 % efficient perovskite quantum-dot-sensitized solar cell. *Nanoscale*. 2011;3:4088–93.
- Etgar L, Gao P, Xue ZS, Peng Q, Chandiran AK, Liu B, et al. Mesoscopic  $\text{CH}_3\text{NH}_3\text{PbI}_3/\text{TiO}_2$  heterojunction solar cells. *J Am Chem Soc*. 2012;134:17396–9.
- Lee MM, Teuscher J, Miyasaka T, Murakami TN, Snaith HJ. Efficient hybrid solar cells based on meso-structured organometal halide perovskites. *Science*. 2012;338:643–7.
- Kim HS, Lee CR, Im J-H, Lee K-B, Moehl T, Marchioro A, et al. Hysteresis and transient behavior in current–voltage measurements of hybrid-perovskite absorber solar cells. *Sci Rep*. 2012;2:1–7.
- Boix PP, Nonomura K, Mathews N, Mhaisalkar SG: Current progress and future perspectives for organic/inorganic perovskite solar cells. *Mater. Today* 2014;17:16–23.
- Heo JH, Im SH, Noh JH, Mandal TN, Lim CS, Chang JA, et al. An easy-to-fabricate low-temperature  $\text{TiO}_2$  electron collection layer for high efficiency planar heterojunction perovskite solar cells. *Nat Photonics*. 2013;7:486–91.
- Burschka J, Pellet N, Moon S-J, Humphry-Baker R, Gao P, Nazeeruddin MK, et al. Sequential deposition as a route to high-performance perovskite-sensitized solar cells. *Nature*. 2013;499:316–9.
- Liu M, Johnston MB, Snaith HJ. Efficient planar heterojunction perovskite solar cells by vapour deposition. *Nature*. 2013;501:395–8.
- McGehee MD. Materials science: fast-track solar cells. *Nature*. 2013;501:323–5.
- Ryu S, Noh JH, Jeon NJ, Kim YC, Yang WS, Seo J, et al. Voltage output of efficient perovskite solar cells with high open-circuit voltage and fill factor. *Energy Environ Sci*. 2014;7:2614–8.
- Xing GC, Mathews N, Sun S, Lim SS, Lam YM, Grätzel M, et al. Long-range balanced electron- and hole-transport lengths in organic–inorganic  $\text{CH}_3\text{NH}_3\text{PbI}_3$ . *Science*. 2013;342:344–7.
- Stranks SD, Eperon GE, Grancini G, Menelaou C, Alcocer MJP, Leijtens T, et al. Electron–hole diffusion lengths exceeding 1 micrometer in an organometal trihalide perovskite absorber. *Science*. 2013;342:341–4.
- Jeon NJ, Lee HG, Kim YC, Seo J, Noh JH, Lee J, et al. *o*-Methoxy substituents in spiro-OMeTAD for efficient inorganic–organic hybrid perovskite solar cells. *J Am Chem Soc*. 2014;136:7837–40.
- Eperon GE, Stranks SD, Menelaou C, Johnston MB, Herz LM, Snaith HJ. Formamidinium lead trihalide: a broadly tunable perovskite for efficient planar heterojunction solar cells. *Energy Environ Sci*. 2014;7:982–8.
- Kojima A, Teshima K, Shirai Y, Miyasaka T. Organometal halide perovskites as visible-light sensitizers for photovoltaic cells. *J Am Chem Soc*. 2009;131:6050.
- Jeon NJ, Noh JH, Kim YC, Yang WS, Ryu S, Seok SI. Solvent engineering for high-performance inorganic–organic hybrid perovskite solar cells. *Nat Mater*. 2014;13:897–903.
- Jeon NJ, Noh JH, Yang WS, Kim YC, Ryu S, Seo J, et al. Fabrication of metal-oxide-free  $\text{CH}_3\text{NH}_3\text{PbI}_3$  perovskite solar cells processed at low temperature. *Nature*. 2015;517:476–80.
- Ball JM, Lee MM, Hey A, Snaith HJ. Low-temperature processed meso-structured thin-film perovskite solar cells. *Energy Environ Sci*. 2013;6:1739–43.
- Liu D, Kelly TL. Perovskite solar cells with a planar heterojunction structure prepared using room-temperature solution processing techniques. *Nature Photon*. 2014;8:133–8.
- Chen Q, Zhou H, Hong Z, Luo S, Duan HS, Wang SH, et al. Planar heterojunction perovskite solar cells via vapor-assisted solution process. *J Am Chem Soc*. 2014;136:622–625.
- Bi D, Moon S-J, Haggman L, Boschloo G, Yang L, Johansson EMJ, et al. Using a two-step deposition technique to prepare perovskite ( $\text{CH}_3\text{NH}_3\text{PbI}_3$ ) for thin film solar cells based on  $\text{ZrO}_2$  and  $\text{TiO}_2$  mesostructures. *RSC Adv*. 2013;3:18762–66.
- Zhou H, Chen Q, Li G, Luo S, Song TB, Duan HS, et al. Photovoltaics. Interface engineering of highly efficient perovskite solar cells. *Science*. 2014;345:542–6.
- Agiorgousis ML, Sun YY, Zeng H, Zhang S. Strong covalency-induced recombination centers in perovskite solar cell material  $\text{CH}_3\text{NH}_3\text{PbI}_3$ . *J Am Chem Soc*. 2014;136:14570–5.
- Cook S, Ohkita H, Kim Y, Benson-Smith JJ, Bradley DDC, Durrant JR. A photophysical study of PCBM thin films. *Chem Phys Lett*. 2007;445:276–80.
- Wei J, Zhao Y, Li H, Li G, Pan J, Xu D, et al. Hysteresis analysis based on the ferroelectric effect in hybrid perovskite solar cells. *J Phys Chem Lett*. 2014;5:3937–45.
- Ono LK, Raga SR, Wang S, Kato Y, Qi Y. Temperature-dependent hysteresis effects on perovskite-based solar cells. *J Mater Chem A*. 2015;3:9074–80.
- McGehee MD. Perovskite solar cells: continuing to soar. *Nature Materials*. 2014;13:845–6.
- Unger EL, Hoke ET, Bailie CD, Nguyen WH, Bowring AR, Heumüller T, et al. Hysteresis and transient behavior in current–voltage measurements of hybrid-perovskite absorber solar cells. *Energy Environ Sci*. 2014;7:3690–8.

Submit your manuscript to a SpringerOpen® journal and benefit from:

- Convenient online submission
- Rigorous peer review
- Immediate publication on acceptance
- Open access: articles freely available online
- High visibility within the field
- Retaining the copyright to your article

Submit your next manuscript at ► [springeropen.com](http://springeropen.com)